

Diese Arbeit wurde vorgelegt am Aerodynamischen Institut

# Investigations on two-way coupling effects of particle-laden decaying isotropic turbulent flows

---

PROJEKTARBEIT  
VON  
JULIAN STEMMERMAN, STEFFEN TRIENEKENS  
UND CHRISTIAN SOIKA

---

Aerodynamisches Institut der RWTH Aachen

September 19, 2017

Betreuer: Konstantin Fröhlich

Erstprüfer: Univ.-Prof. Dr.-Ing. Wolfgang Schröder

# Contents

<b>1</b>	<b>Nomenclature</b>	<b>2</b>
<b>2</b>	<b>Introduction</b>	<b>3</b>
<b>3</b>	<b>Mathematical models</b>	<b>4</b>
3.1	Single-phase flow . . . . .	4
3.1.1	The Navier-Stokes equations . . . . .	4
3.1.2	Turbulent flows: Across all scales . . . . .	6
3.2	Particle dynamics . . . . .	8
<b>4</b>	<b>Numerical methods</b>	<b>11</b>
4.1	Direct numerical simulation . . . . .	11
4.2	Large-eddy simulation . . . . .	11
4.3	Discretisation . . . . .	12
4.4	Particle clustering . . . . .	12
<b>5</b>	<b>Results</b>	<b>13</b>
<b>6</b>	<b>Conclusion and outlook</b>	<b>16</b>
<b>7</b>	<b>References</b>	<b>17</b>

# 1 Nomenclature

$\eta$	Kolomogorov scale	$\mathbf{q}$	Heat conduction
$\boldsymbol{\tau}$	Stress tensor	$\mathbf{u}$	Three-dimensional velocity
$\mathbf{I}$	Identity tensor	$\mathbf{v_p}$	Particle velocity
$\mathbf{S}$	Rate-of-strain-tensor	$\mathbf{v}$	particle velocity
$\mu$	Dynamic viscosity	$\mathbf{x_p}$	Particle position
$\rho$	Density	$\mathbf{x}$	particle position
$\rho_p$	Particle density	$c_p$	Specific isobaric heat capacity
$\tau_{mp}$	Particle response time	$c_v$	Specific isochoric heat capacity
$\nabla$	Nabla-operator	$E$	Specific inner energy
$\mathbf{a}$	particle acceleration	$e$	Specific internal energy
$\mathbf{H^i}$	Stores the inviscid variables in the flux-vector included in the Navier-Stokes equations	$f_{mD}$	Drag correction
$\mathbf{H^v}$	Stores the viscous variables in the flux-vector included in the Navier-Stokes equations	$k_t$	thermal conductivity
$\mathbf{H}$	Container for fluctuating variables in the Navier-Stokes equations	$m_c$	number of clustered particles
$\mathbf{Q}$	Container for conserved variables in the Navier-Stokes equations	$p$	Pressure
		$Pr$	Prandtl number
		$R$	Universal gas constant
		$r_p$	Particle radius
		$Re$	Reynolds number
		$S$	Sutherland temperature
		$T$	Temperature

## 2 Introduction

in Computational Methods for Multiphase Flow ist auf den Seiten 3-9 ein interessantes Beispiel. Sollen wir hier außerdem noch ein Bild von einer turbulenten Strömung und der Sammlung der Partikel in low-vortex-areas einfügen? Unterschiedliche Sections erklären Einführung von  $m_c$  beschreiben. Ablauf: 1. Beispiel für technische Anwendungen 2. Inhalt der Arbeit zusammenfassen

### 3 Mathematical models

#### 3.1 Single-phase flow

In this section the mathematical basics for understanding and simulating turbulent flows are discussed. However, it should be pointed out that this is no complete treatise of the mathematical and physical basics. The reader can achieve further insight on this topic by looking at different books and papers, e.g. [9].

##### 3.1.1 The Navier-Stokes equations

The Navier-Stokes-Equations are of great importance for understanding turbulent phenomena. This set of equations exists in forms for compressible and incompressible fluids. For an infinitesimal small volume element  $d\tau$  and using the cartesian coordinate system, they can be written in the so-called 'divergence form':

$$\frac{\partial \mathbf{Q}}{\partial t} + \nabla \mathbf{H} = 0 \quad (3.1)$$

The vector  $\mathbf{Q}$  contains all the variables which are conserved, i.e. the density  $\rho$ , the velocity  $\mathbf{u}$  and the specific inner energy  $E$ :

$$\mathbf{Q} = \begin{pmatrix} \rho \\ \rho \mathbf{u} \\ \rho E \end{pmatrix} \quad (3.2)$$

$\mathbf{H}$  is the flux vector which stores all the floating variables and may be split up into two parts:

$$\mathbf{H} = \mathbf{H}^i + \mathbf{H}^v \quad (3.3)$$

The contents of the two vectors are displayed below:

$$\mathbf{H}^i = \begin{pmatrix} \rho \mathbf{u} \\ \rho \mathbf{u} \mathbf{u} + p \\ \mathbf{u}(\rho E + p) \end{pmatrix} \quad (3.4)$$

$$\mathbf{H}^v = -\frac{1}{Re} \begin{pmatrix} 0 \\ \boldsymbol{\tau} \\ \boldsymbol{\tau} \mathbf{u} + \mathbf{q} \end{pmatrix} \quad (3.5)$$

$\mathbf{H}^i$  is called inviscid flux and contains only the variables that are independent of the fluids viscosity, it describes the way a fluid with zero viscosity would behave. In contrast, the viscous flux  $\mathbf{H}^v$  represents the effects of viscosity. The Reynolds

number  $Re = \frac{\rho v d}{\eta}$  is defined to be the ratio of inertia to tenacity, which makes it very valuable for understanding turbulent flows. This is also due to the fact that two familiar objects with the same Reynolds number behave similar in turbulence. One can assume that flows with  $Re \ll 1$  are laminar and flows with  $Re \gg 1$  are turbulent. To solve the Navier-Stokes-Equations, more information regarding some variables is required. For Calculating the specific inner Energy  $E$  and the heat conduction  $\mathbf{q}$ , the following equations are used:

$$E = e \frac{1}{2} |\mathbf{u}|^2 \quad (3.6)$$

$$\mathbf{q} = -\frac{\mu}{Pr(\gamma - 1)} \nabla T \quad (3.7)$$

with

$$\gamma = \frac{c_p}{c_v} \quad (3.8)$$

and the Prandtl number

$$Pr = \frac{\mu_\infty c_p}{k_t} \quad (3.9)$$

using the specific heat capacities of the fluid  $c_v$  and  $c_p$ . If one could assume that the fluid is a newtonian fluid, the linear correlation between stress and the rate of strain results in:

$$\boldsymbol{\tau} = 2\mu \mathbf{S} - \frac{2}{3}\mu(\nabla * \mathbf{u})\mathbf{I} \quad (3.10)$$

in which  $\mathbf{S} = \frac{(\nabla \mathbf{u})(\nabla \mathbf{u})^T}{2}$  denotes the rate-of-strain-tensor. Additionally, the viscosity  $\mu$  can be approximated through Sutherland's law, which is based on the ideal gas-theory:

$$\mu(T) = \mu_\infty \left(\frac{T}{t_\infty}\right)^{3/2} \frac{T_\infty + S}{T + S} \quad (3.11)$$

$S$  is in this case the Sutherland temperature. To achieve closure the caloric state equation  $e = c_v T$  and the state equation for an ideal gas  $p = \rho R T$  are used. The specific gas constant is determined by  $R = c_p - c_v$ . These equations form a set of partial differential equations, so for solving them starting values are needed.

### 3.1.2 Turbulent flows: Across all scales

Turbulent flows contain eddies of all sizes and forms. Large-scale eddies bring energy to the flow which is then passed down to smaller-scale eddies and in the end dissipated into heat by viscous effects. This behavior is called the 'energy cascade' and was first described by Richardson in the year 1922. The theory then was developed further by Kolmogorov and published 1941.

The first set of scales describe the large eddies. These scales are called *integral* scales and are determined by the physical boundaries of the flow. As said before, at these scales the energy is brought into the flow, creating the so-called 'energy-containing range'. The length scale is the called integral length scale  $L$ , and the corresponding timescale which is most times called 'eddy turnover time' is defined as:

$$\tau_L = \frac{L}{U} \quad (3.12)$$

where  $U$  denotes the characteristic velocity.

The smallest scales in a turbulent flow are the Kolmogorov length ( $\eta$ ) and time ( $\tau_\eta$ ) scale. At this scales, the effects of viscosity take place and the energy dissipates into heat. With the estimate  $\epsilon \sim \frac{U^3}{L}$  they can be written as

$$\eta = \left( \frac{\nu^3 L}{U^3} \right)^{1/4} \quad (3.13)$$

$$\tau_\eta = \left( \frac{\nu L}{U^3} \right) \quad (3.14)$$

Both these scales are coupled by the Reynolds number:

$$\frac{L}{\eta} = Re^{3/4} \quad (3.15)$$

$$\frac{\tau_L}{\tau_\eta} = Re_L^{1/2} \quad (3.16)$$

It can be seen from these two equations that the difference between the scales increases for higher Reynolds numbers.

A scale between these two is the Taylor microscale, often referred to as 'turbulence length scale'. Although it lacks of a physical interpretation, it is often used to describe the intermediate range between integral and Kolmogorov scales. Its definition is:

$$\lambda = \sqrt{15 \frac{\nu}{\epsilon}} |\mathbf{v}'| \quad (3.17)$$

with  $|\mathbf{v}'|$  denoting the absolute value of the velocities fluctuation. This scale can be used to compute another Reynolds number  $Re_\lambda$ :

$$Re_\lambda = \frac{|\mathbf{v}'| \lambda}{\nu} \quad (3.18)$$

Together these scales form a powerful tool to understand and compute turbulent flows.



### 3.2 Particle dynamics

Siewert: -3.1a-3.14 (spherical particles) OHNE GRAVITATION Stokes Drag/Stokes Coefficient Filterung (Fritz) - Viskosität durch numerischen Fehler, Smagorinsky nicht benutzen

Since this work deals with particle laden fluids and the impact of these particles on the flow conditions, we need to describe the interaction between them. We deal with small and heavy, rigid particles, that have a spherical shape. Their radius  $r_p$  is even smaller than the Kolmogorov scale  $\eta$ , but also large enough to neglect the Brownian motion. Due to the small particle concentration, the best and most common way to describe these flows is the point particle approach, which means that every particle is treated as an mathematical point source of mass, momentum and energy. In this case we focus on the momentum exchange. Effects like particle-particle interactions, particle-wall interactions are also neglected. At describing the motion of the particles in the following the fact, that we deal with gas-solid flows is an advantage, since we can make several simplifications. First we look at the influence of the particles on the carrier fluid. Here we make the assumption, that the fluid is incompressible and the mass exchange over the particle surface is zero. Hence the continuity equation becomes:

$$\nabla \cdot \mathbf{u} = 0 \quad (3.19)$$

. The Navier Stokes equation, described in chapter 1, becomes:

$$\rho \frac{D\mathbf{u}}{Dt} = -\nabla p + \nabla \cdot \boldsymbol{\tau} + \mathbf{F} \quad (3.20)$$

The influence of the particles on the fluid is represented by the new term  $\mathbf{F}$ , which describes the force per unit volume on the fluid. We could approximate  $\mathbf{F}$  by a superposition of Dirac's delta functions over all particles, centered at the location  $\mathbf{x}_p^n$  of each particle:

$$\mathbf{F} = \sum_n \mathbf{f}^n \delta(\mathbf{x} - \mathbf{x}_p^n) \quad (3.21)$$

$\mathbf{x}_p^n$  is the position of the n-th particle and results from the kinematic equation

$$\frac{d\mathbf{x}_p}{dt} = \mathbf{v}_p \quad (3.22)$$

$\mathbf{v}_p$  is the velocity of the n-th particle.  $\mathbf{f}^n$  is the sum of forces acting between fluid and particles. Hence it plays also an important role in the equation of motion of the particles:

$$\rho_p \frac{d\mathbf{v}_p}{dt} = \rho_p \mathbf{g} + \mathbf{f}^n(\mathbf{x}_p^n) \quad (3.23)$$

As already mentioned  $\mathbf{f}^n(\mathbf{x}_p^n)$  could be divided in several forces. Then the equation of motion looks like:

$$v_v * \rho_p * \frac{\partial \mathbf{v}_p^n}{\partial t} = v_v * \rho_p * \mathbf{g} + \mathbf{f}_d + \mathbf{f}_l + \mathbf{f}_a + \mathbf{f}_h + \mathbf{f}_{\text{additional}} \quad (3.24)$$

Here  $\mathbf{f}_d$  represents the hydrodynamical drag force that is parallel to the undisturbed streamlines, which depends on an empirical drag coefficient  $C_d$ :

$$\mathbf{f}_d = -\frac{3}{4} * \rho * v_v * \frac{C_d}{d} * |\mathbf{v}_p - \mathbf{u}| * (\mathbf{v}_p - \mathbf{u}) \quad (3.25)$$

$\mathbf{u}$  is the velocity of the uniform stream, which is enough away from the particle that it is undisturbed from the particle. The other partial hydrodynamical force, the lift force  $\mathbf{f}_l$  is perpendicular to the undisturbed streamlines. Furthermore the added mass force  $\mathbf{f}_a$  represents the influence of the inertia of the fluid that has an impact on the particle, if it has a different acceleration than the mean flow. Hence it could be determined by:

$$\mathbf{f}_a = \frac{1}{2} * \rho * v_v * \left( \frac{D * \mathbf{u}}{D * t} - \frac{d * \mathbf{v}_p}{d * t} \right) \quad (3.26)$$

——-nie  $\mathbf{v}$  sondern immer  $\mathbf{v}_p$  benutzen——- The history force  $\mathbf{f}_h$  takes diffusion and convection, that results out of the vortices behind the particles, into account. We look at Basselt's result, neglecting the finite size correction that is proportional to  $\nabla^2 * \mathbf{u}$ :

$$\mathbf{f}_h = \frac{3}{2} * d^2 * \rho * \sqrt{\pi * \nu} * \int_t^0 \frac{dt'}{(t - t')^{1/2}} \left( \frac{D\mathbf{u}}{Dt'} - \frac{d\mathbf{v}_p}{dt'} \right) \quad (3.27)$$

In our case of gas-solid suspensions we can make several simplifications. In the following we show with an rough approximation that the added mass and history forces are negligible compared with the drag force. We use the approach that the relative velocity is of the same order as the terminal velocity  $v_t$ . The terminal velocity is the velocity of a particle in a resting fluid, when gravitation and drag force are in equilibrium. Then if the added mass and the drag force are compared, we get the following equation:

$$\frac{|\mathbf{f}_a|}{|\mathbf{f}_d|} \simeq \frac{\frac{1}{2} * \rho * v_v * g}{\frac{3}{4} * \rho * v_v * (C_d/d) * v_t^2} \frac{a_r}{g} = \frac{1}{2} * \frac{\rho}{\rho_p} * \frac{a_r}{g} \quad (3.28)$$

with

$$a_r = \left( \frac{D\mathbf{u}}{Dt} - \frac{d\mathbf{v}_p}{dt} \right) \quad (3.29)$$

Since in gas-solid suspensions the particle density is of an factor of 1000 higher than the fluid density, it shows that, if it's not the unlikely case that the relative acceleration is of the same order higher than the gravity, the added mass force is

negligible compared to the drag force. The effect that fluid and particle influence each other is called two-way-coupling.  $\mathbf{f_d}$  and lift forces,  $\mathbf{f_a}$  the added mass and  $\mathbf{f_h}$  the history forces. The last term  $\mathbf{f_{additional}}$  is attached for the case that we have to take other forces like electrostatic interactions into account.

-coupling Zahl

The relaxation time  $\tau_p$  physically represents the time scale over which the drag force decreases the particle relative velocity to zero and is determined by the following equation:

$$\tau_p = \frac{\rho_p}{\rho_f} * \frac{2 * r_p^2}{9 * \nu} \quad (3.30)$$

Since we consider gas-solid flows, which means we can use a point particle approach make some simplifications in the following To get a useful equation of motion for the particles in the flow, we use the Euler Lagrangian approach, as it is common in Direct Numerical Simulations (DNS) and Large Eddy Simulations (LES). The density of the particles  $\rho_p$  is much higher than that of the fluid  $\rho_f$ . In addition due to the very low particle concentration we can neglect the influence of the particles on each other. That means that they cross each other without any effect. That means particle collision is neglected. After all these simplifications we obtain a simplified version of the Maxey-Riley equations.

$$\frac{\partial \mathbf{x}_p}{\partial t} = \mathbf{v}_p \quad (3.31)$$

$$\frac{\partial \mathbf{v}_p}{\partial t} = \frac{f_D}{\tau_p} (\mathbf{u}(\mathbf{x}_p) - \mathbf{v}_p) \quad (3.32)$$

$\tau_p$  is the particle response time and a factor to obtain the drag force in Stokes flow conditions. To take the case of a Reynolds number  $\mathcal{R}$  of order 1 into account the correction factor  $f_D = 1 + 0.15Re_p^{(0.687)}$  is used. The biggest simplification of this Lagrangian approach is that the interaction of particles coming close together is neglected.

## 4 Numerical methods

To simulate flows like those described above we have two options. The direct numerical simulation (DNS) is the easier one to understand, although it is numerically very expensive. The Large-eddy simulation (LES) is numerically more capable, still we must accept certain inaccuracies. These two numerical methods are now discussed in the following chapter.

### 4.1 Direct numerical simulation

The basis of the direct numerical simulation (DNS) are the Navier-Stokes equations as described above. The idea is that the computer is very good at calculating and solves these equations completely. This provides a very accurate result, as all scales of motion are being resolved. Still it requires an immense level of computational resources which increases rapidly with the Reynolds number. These computational resources were not available until the 1970s. Even though it is not advisable to resolve every scale of motion, if only the contained energy is of greatest interest. With the large-eddy simulation, as described below, the computational effort is 99.98 % less compared to DNS, which indeed is the fraction of the dissipative scale. This leaves 0.02 % of the flow, which is correlative with the fraction of the energy-containing larger-scale [9].

### 4.2 Large-eddy simulation

Due to the fact that DNS is effortful and wasting resources if a fully resolved resolution is not required, large-eddy simulation (LES) was created to save time and resources. This is especially efficient if mainly the temporal energy trend is considered, because the energy containing larger-scale motion is completely resolved and the indeed small effects of the expensive smaller-scale motion are just modelled. Otherwise in DNS resolving the small dissipative scale would require most of the computational resources.

Simulating only the larger-scale motions is also called filtering, which means that the smaller-scale motions are filtered out. To model the filtered smaller-scale motions usually a subgrid-scale (SGS) model is used. According to Hickel (2007) the interference between explicit SGS and the truncation error can be exploited, i.e. the truncation error can serve as model of the effects of unresolved scales, which is therefore an implicit SGS model. Thus we call it implicit LES (ILES) [6].

### 4.3 Discretisation

To integrate the Lagrangian particle tracking equations, discussed above, a predictor-corrector scheme based on the trapezoidal rule for numerical integration

$$f(t + \delta t) \approx f(t) + \frac{\delta t}{2} \left[ \frac{\partial f(t)}{\partial t} + \frac{\partial f(t + \delta t)}{\partial t} \right] \quad (4.1)$$

is used.

The first step is the prediction of the new particle position  $\mathbf{x}_{n+1}^{(p)}$  using a Taylor expansion for a small time step  $\delta t$

$$\mathbf{x}_{n+1}^{(p)} = \mathbf{x}_n + \delta t \mathbf{v}_n + \frac{1}{2} \delta t^2 \mathbf{a}_n. \quad (4.2)$$

Due to the computational effort we will put  $\mathbf{u}_{n+1}^{(p)}$  on the level of the nearest cell fluid velocity.

The updated velocity and acceleration are calculated as

$$\mathbf{v}_{n+1} = \frac{\mathbf{v}_n + \frac{1}{2} \delta t \left( \mathbf{a}_n + \frac{f_D}{\tau_p} \mathbf{u}_{n+1}^{(p)} + \mathbf{g} \right)}{1 + \frac{1}{2} \frac{f_D}{\tau_p} \delta t}, \quad (4.3)$$

$$\mathbf{a}_{n+1} = \frac{\frac{f_D}{\tau_p} \left( \mathbf{u}_{n+1}^{(p)} - \mathbf{v}_n - \frac{1}{2} \delta t \mathbf{a}_n \right) + \mathbf{g}}{1 + \frac{1}{2} \frac{f_D}{\tau_p} \delta t}. \quad (4.4)$$

The updated particle position must be corrected by an additional term according to the trapezoidal rule

$$\mathbf{x}_{n+1} = \mathbf{x}_n + \frac{1}{2} \delta t (\mathbf{v}_{n+1} + \mathbf{v}_n) + \frac{1}{12} \delta t^2 (\mathbf{a}_{n+1} - \mathbf{a}_n). \quad (4.5)$$

### 4.4 Particle clustering

The high number of point particles require even more computational resources for the particle-laden simulation. The main idea to reduce this requirement is to create clusters of point particles, meaning that a new variable  $m_c$  is introduced. We consider a cluster of  $m_c$  point particles as one larger point particle, i.e. the program has less particles to simulate. To compensate this lack of particles, the coupling force is multiplied by  $m_c$ , due to the  $m_c$ -fold mass of the (cluster-)particles. In chapter 5 (results) we evaluate the legitimacy of particle clustering and the maximum acceptable value of  $m_c$ .

Projektion (noComputationalParticles), Diskretisierung implizite LES (Motivation fuer LES - Pope Chapter 9, Bild 9.4), DNS

## 5 Results

The simulations were carried out using ZFS, the simulation tool developed and implemented at the Institute of Aerodynamics at RWTH Aachen University [1] [2]. The tool is capable of simulating finite-volume flows of compressible fluids. In this case the turbulence was simulated on a cubic grid using  $64^3$ ,  $96^3$ ,  $128^3$  and  $256^3$ . The first three cases were simulated using LES, the case in which  $256^3$  cells were used is carried out as DNS. Further information can be gained by looking at [9, p.344-357 for DNS and p. 558-639 for LES].

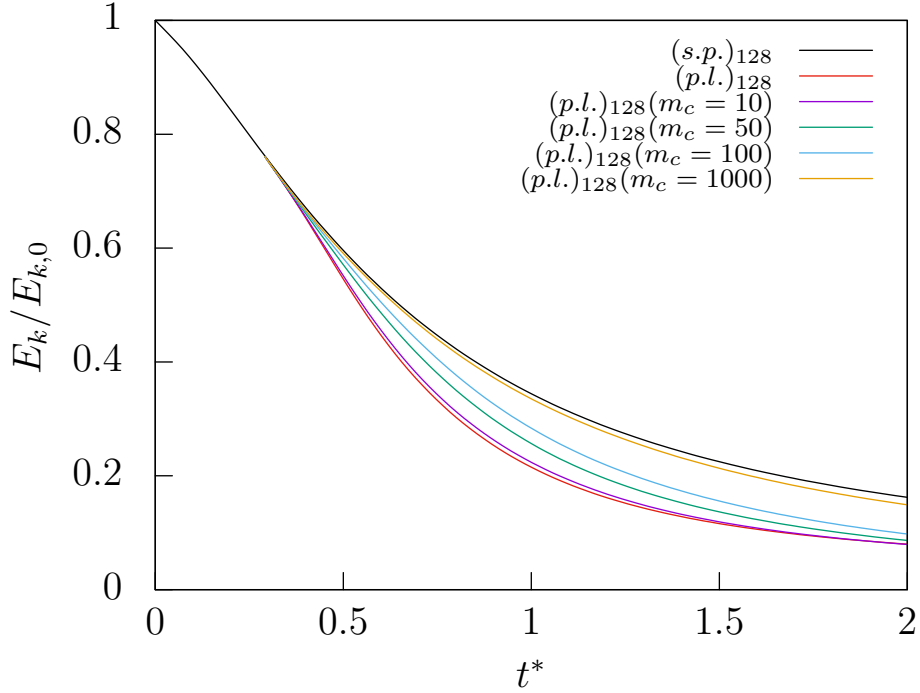


Figure 1: Kinetic Energy over eddy turnover times for different numbers of particles

For simplification, the special case of isotropic turbulence was used. For this idealised flow form the statistical velocities are invariant in all directions of the grid. It follows that the flows velocity are invariant for rotations and reflections. The turbulence was initialised using a seed-based random generator. To achieve physical results, the simulation of the particle-free flow was carried out to timestep 150, at which a restart file was written out. This procedure ensures a fully developed turbulent flow, whom has emancipated from the initialisation. In this flow field, a specific number of spherical particles were injected.

As noted in [7], particles tend to cluster in certain regions of the turbulent flow. This behavior can be used to minimize computational effort for simulating the

flow while still achieving high quality results. To investigate the differences in accuracy for different sizes of particles, the variable  $m_c$  was introduced to the code describing the number of particles in one cluster. The simulations were then set up with the overall same number of particles ( $10^6$ ), just the number of particles in one cluster was altered. Then the simulations were carried out normally and result in the following graphs (Figure 1, 2 and 3). It can be seen in figure 1 that the decay in kinetic energy from the starting point depends highly on the number of clustered particles. **With 10 particles per cluster, the solutions could be usable to get a first impression for technical purposes, all other simulations show a very high variety.**

Fitting to this first results, the Graphs of figure 2 and 3 clearly show that for sim-

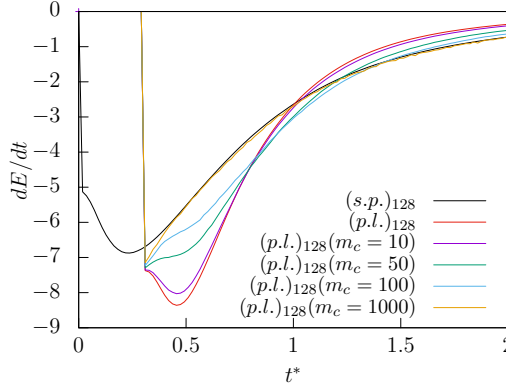


Figure 2: Change in kinetic Energy over eddy turnover times

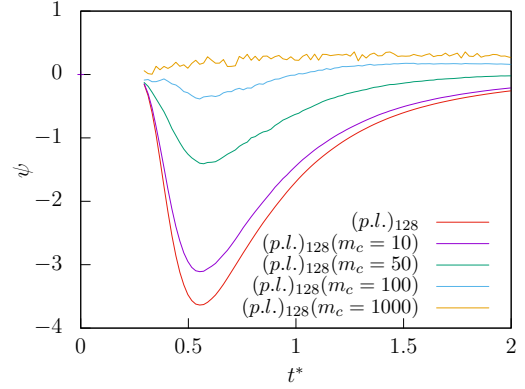


Figure 3: Coupling Rate over eddy turnover times

ulations with highly clustered particles the simulations results differ a lot. Looking at the results for the change in kinetic Energy, the difference becomes evident: The lower  $m_c$  is, the higher is the drop in kinetic Energy. This behavior can be seen because of the particles initially 'soaking up' energy, then in later phases of the flow giving it back in form of their inertia and speed, which they gathered in the beginning. **This effect should grow bigger by particle size and weight.** This change in energy transfer occurs at the unclustered simulation at about one eddy turnover time. In cases with more clustered particles it occurs later, only the case in which 1000 particles were clustered shows a strange behavior. It catches up the particle-free case very fast, which leads to the conclusion that the amount of clusters is so small that the flow almost behaves like one without particles. Additionally the change in kinetic Energy shows inconstancy which can also be traced back to the small cluster number. The amount is just too small to achieve high-quality information in the statistical variables.

The same impression can be achieved by looking at the graphs describing the coupling rate. The particle-laden-case makes the biggest jump into negative coupling rate. The higher the amount of coupled particles, the lower is the negative coupling rate. This evolution continues until the physicality vanishes and the randomness starts to show at the results for  $m_c$  higher than 50.

The properties of these simulations can be found in table 1 on page 15. The ratio of the densities was set to  $\frac{\rho_p}{\rho} = 1000$ . At the timestep of injection the particle response time  $\tau_p = \frac{d^2}{18\nu} \frac{\rho_p}{\rho}$  was 0.03497 **Uebepruefen, ist die Viskositaet die richtige?**.

$m_c$	$u_0$	$\epsilon$	$\lambda$	$\eta$	$Re_\lambda$
1	0.7628	5.22897	0.0317221	0.00207819	60.1557
10	0.7628	5.22927	0.0317214	0.00207816	60.1547
50	0.76282	5.23008	60.1512	0.0020780	60.1512
100	0.76286	5.23117	0.0317167	0.00207797	60.148
1000	0.76301	5.2359	0.0317056	0.00207751	60.1329

Table 1: Variables of the first set of simulations at the time of injection for  $128^3$ -case

To find out at which number of particles the results are sufficiently exact, a second set of simulations was carried out. As mathematics of turbulent flows are based on averaged variables, small numbers of particles can lead to false and even unphysical results. In these simulations, no particle clustering was used, just different amount of particles were injected into the same flow. For these simulations similar properties to the ones from the first set of simulations were used, just the mentioned number of particles was changed. The results can be seen on page 16 on figure 4. The normalized difference in **kinetic Energy** shows in this one-time simulation a clear correlation between particle number and accuracy in the simulation. Although this was just a single initialization of particles in a flow, it can be stated that simulations using only  $10^2$ ,  $10^3$  or even up to  $10^4$  particles are not accurate enough for technical or scientific use of the data. One-time simulations in other gridsizes show similar results.



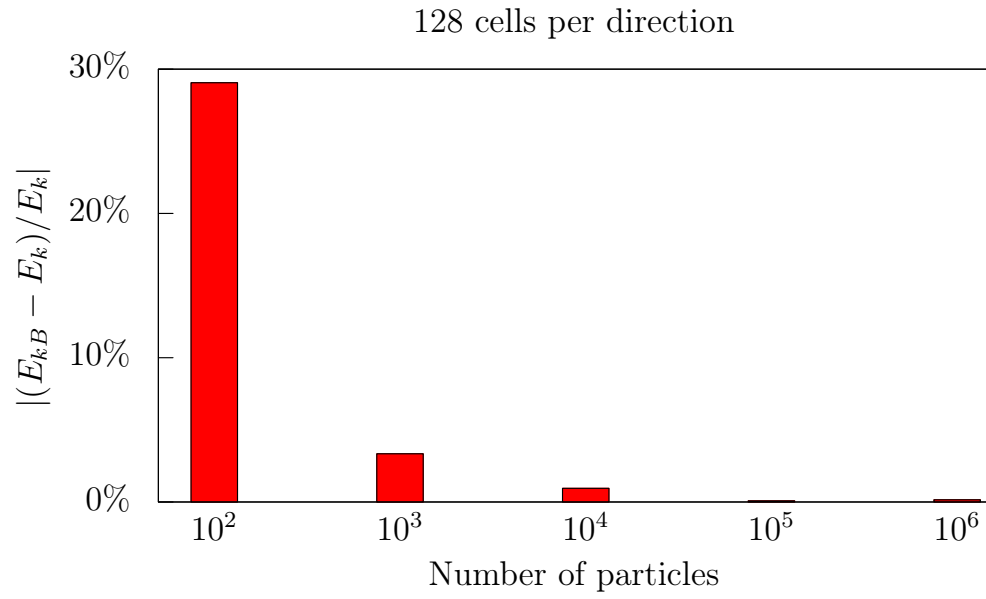


Figure 4: Results for initializing different numbers of particles

## 6 Conclusion and outlook

Offene Themen: Statistische Auswertung der Anzahl der Partikel (Konvergenz)

### Acknowledgements

## 7 References

- [1] W. Schröder D. Hartmann, M. Meinke. An adaptive multilevel multigrid formulation for cartesian hierarchical grid methods. *Comput. Fluids*, 2008.
- [2] W. Schröder D. Hartmann, M. Meinke. A strictly conservative cartesian cut-cell method for compressible viscous flows on adaptive grids. *Comput. Meth. Appl. Mech. Eng.*, 2010.
- [3] S. Elghobashi. Particle-laden turbulent flows: direct simulation and closure models. *Applied Scientific Research*, 1991.
- [4] S. Elghobashi. On predicting particle-laden turbulent flows. *Applied Scientific Research*, 1993.
- [5] S. Fritz. Simulation isotroper turbulenz. study work, 2003.
- [6] S. Hickel. *Implicit Turbulence Modeling for Large-Eddy Simulation*. PhD thesis, Technische Universität München, 2007.
- [7] John K. Eaton John R. Fessler, Jonathan D. Kulick. Preferential concentration of heavy particles in a turbulent channel flow. *Physics of Fluids*, 1994.
- [8] M. Meinke K. Fröhlich, L. Schneiders and W. Schröder. Validation of particle-laden large-eddy simulation using hpc systems. In *Sustained Simulation Performance 2017*, 2017. unpublished conference document.
- [9] S. B. Pope. *Turbulent Flows*. Cambridge University Press, 2010.
- [10] A. Prosperetti and G. Tryggvason. *Computational Methods for Multiphase Flow*. Cambridge University Press, 2009.
- [11] W. Schröder. Fluidmechanik. lecture notes 'Fluid mechanics', 2010.
- [12] C. Siewert. *Numerical Analysis of Particle Collisions in Isotropic Turbulence*. PhD thesis, RWTH Aachen University, 2014.